Chapter 5 CO2 gas coolers and cooling processes

Yunting Ge

Abstract

CO_2 gas coolers are widely applied in CO_2 refrigeration, air conditioning and heat pump systems. The controls, operations, modelling and designs of the CO_2 gas coolers are important to the performance of their associated systems and thus are discussed extensively in this chapter. For the controls, it is explained the reason for the existence of optimal heat rejection pressure and how to predict and control the optimal pressure at different operating conditions. For the operations of cooling processes, some important correlations from literatures for the heat transfer and hydraulic calculations are introduced and discussed. In addition, different modelling methods for the gas cooler performances are discussed and compared. The modelling with distributed method is purposely introduced together with model validations and simulation results. Furthermore, the application of CO_2 gas coolers in automobile is explained and some design options are recommended.

5.1 Optimal heat rejection pressure

Compared to conventional HFC refrigerants such as R134a in vapour compression systems, the most extraordinary thermophysical properties of the CO_2 working fluid are its low critical temperature of 31.1°C and extremely high critical pressure of 7.38 MPa. In such circumstances, for a CO_2 refrigeration or heat pump system, if the temperature of a heat rejection medium such as ambient air or cooling water is relatively high, there will be no condensation during the high pressure heat rejection process. Considering the essential low pressure evaporation process in the system, the CO_2 heat rejection process at the high pressure side will subsequently operate at supercritical cooling process starting from the compressor outlet. After that, the refrigerant flow will undergo the processes of expansion, evaporation and compression. In that case, the heat exchanger for the CO_2 heat rejection will be called CO_2 gas cooler instead of CO_2 condenser. The operating supercritical pressure of CO_2 will thus be independent of CO_2 temperature. Meanwhile, the system operates in a transcrtical refrigeration cycle.

A typical CO_2 transcritical refrigeration cycle can be demonstrated in Fig. 1. As depicted, there are four processes in the cycle, including isentropic compression 1-2s by a compressor, isobaric gas cooling 2s-3 by a gas cooler, isenthalpic expansion 3-4 by a thermostatic expansion valve , and isobaric evaporation 4-1 by a evaporator. The evaporator refrigeration effect q_0, compressor specific work w, cooling COP in the cycle, an isothermal line T_{ex} showing the CO_2 temperature at the gas cooler exit and an isentropic line for the compression process are also indicated and demonstrated in the diagram.

At a constant evaporating temperature T_0 , constant CO_2 gas cooler exit temperature T_{ex} and a fixed refrigerant state at the compressor inlet, the refrigeration effect q_0 and compressor specific work w both increase with higher CO_2 pressures at the compressor outlet. However, due to the 'S' shape of the isothermal line T_{ex} and nearly linear shape of the isentropic line, the cooling COP will increase and decrease with the growth of heat rejection pressure. This means that there is an optimal heat rejection pressure in the gas cooler at which the cooling COP is maximised [1-2]. This is different from that of a conventional vapour compression refrigeration cycle with both evaporation and condensation processes in which the cooling COP always decreases with higher condensing pressures. Subsequently, to enhance the performance of a

CO_2 refrigeration or heat pump cycle, an important task is to determine and control the optimal high-side pressure at a specific operating condition.

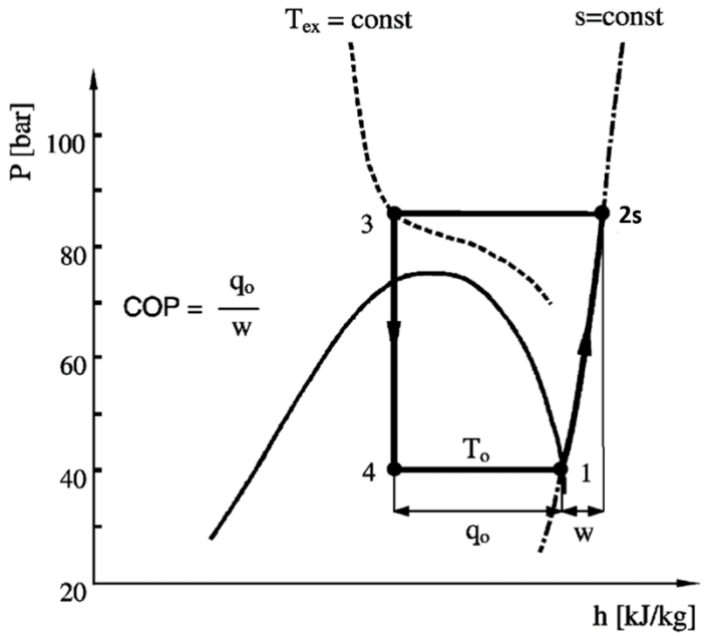

Fig. 1 A simplified CO_2 transcritical refrigeration cycle

5.2. Prediction of optimal heat rejection pressure

In an actual operation of a CO_2 refrigeration or heat pump system, the evaporator evaporating temperature will vary, while the compressor compression process will not be isentropic, and there will be some degrees of superheating at the evaporator outlet or the compressor inlet. In addition, there are some pressure drops during CO_2 gas cooling and evaporation processes. To reflect this, a practical CO_2 transcritical refrigeration cycle is shown in Fig. 2. To simplify the analysis, no pressure drop is assumed for either CO_2 gas cooling (2-3) or evaporation process (4-1). In Fig. 2, point e is at the saturated vapor state along the evaporation line while the dot line 1-2s indicates the isentropic compression process.

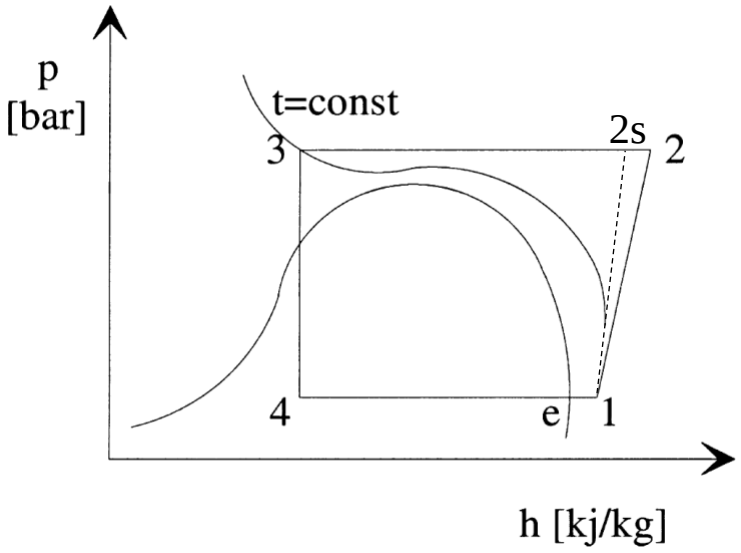

Fig.2 A practical CO_2 refrigeration transcritical cycle

Accordingly, the cooling COP can be calculated as:

$$COP = \frac{h_1 - h_4}{h_2 - h_1} = \frac{h_1 - h_3}{h_2 - h_1} = \frac{h_1 - h_3}{h_{2s} - h_1} \times \eta_{is} \quad (1)$$

The cooling COP is therefore a function of a number of parameters including heat rejection pressure p_{gc}, CO_2 gas cooler outlet temperature t_{ex}, evaporating temperature t_e, superheating at the compressor inlet Δt_{sh} and isentropic efficiency of compressor η_{is}:

$$COP = f(p_{gc}, t_{ex}, t_e, \Delta t_{sh}, \eta_{is}) \quad (2)$$

The optimal heat rejection pressure can be calculated when the COP is maximised and the following equation is satisfied:

$$\left[\frac{\partial COP}{\partial P_{gc}}\right]_{p_{gc}=p_{gc,opt}} = 0 \quad (3)$$

Based on a parametric simulation, superheating Δt_{sh} affects the optimal heat rejection pressure less compared to other parameters [3]. If the isentropic efficiency could be considered as a constant, the optimal pressure will predominantly be the function of the gas cooler outlet temperature and evaporating temperature. Furthermore, of these two parameters, the effect of gas cooler outlet temperature is more significant [4]. As an example, the effects of the gas cooler outlet temperature on the optimal heat rejection pressure and cooling COP are calculated and shown in Fig. 3 . Hence, a lower gas cooler outlet temperature is expected since it leads to higher cooling COP and lower optimal heat rejection pressure. This requires the gas cooler approach temperature to be as small as possible. The approach temperature is defined as the temperature difference between the gas cooler CO_2 outlet temperature and inlet temperature of the heat rejection medium. There are a number of issues which can affect the approach temperatures including the heat exchanger types, designs and heat transfer and hydraulic behaviours of CO_2 flow and heat rejection medium.

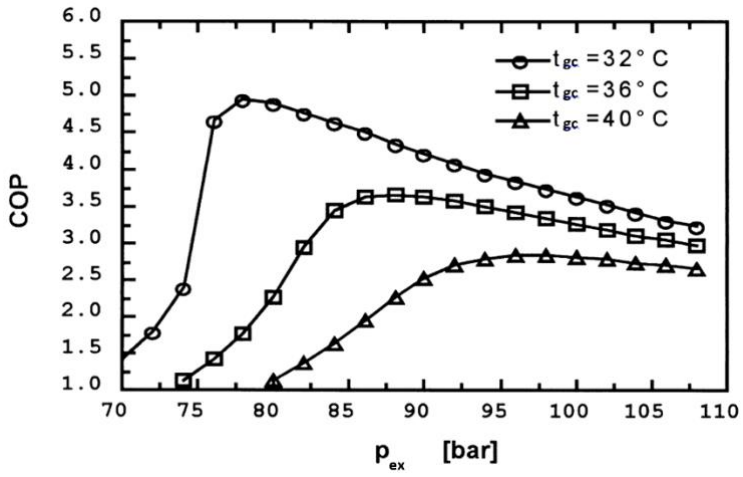

Fig. 3 The effect of CO_2 gas cooler outlet temperature on the optimal heat rejection pressure and cooling COP

5.3 Heat transfer and hydraulic analyses

5.3.1 Heat transfer coefficient

The measurements and correlations of CO_2 heat transfer coefficient and pressure drop for CO_2 gas coolers are mostly on internal supercritical cooling flow with both larger-diameter and microchannel tubes. The term 'microchannel' is used for flow channels with a hydraulic diameter of less than 1 mm.

There are two well-known correlations by Gnielinski [5] and Pitla [6] for the calculations of in-tube supercritical CO_2 gas flow heat transfer coefficients. The Gnielinski correlation is based on Nusselt number that is calculated using the thermophysical properties at the bulk temperature and is calculated as below:

$$Nu = \frac{\xi/8(Re-1000)Pr}{12.7\sqrt{\xi/8}\left(Pr^{\frac{2}{3}}-1\right)+1.07} \tag{4}$$

The friction factor ξ is a function of Reynolds number only and is calculated as the correlation proposed by Krasnochekov et al. [7].

$$\xi = (0.79\ln(Re) - 1.64)^{-2} \tag{5}$$

The Reynolds , Prandtl and Nusselt numbers are calculated in equations (6) ,(7) and (8)respectively.

$$Re = \frac{Gd}{\mu} \tag{6}$$

$$Pr = \frac{\mu C_p}{\lambda} \tag{7}$$

$$Nu = \frac{\alpha d}{\lambda} \tag{8}$$

The heat transfer coefficient α can therefore be calculated.

The Pitla correlation is based on mean Nusselt numbers that are calculated using the thermophysical properties at the wall and bulk temperatures. The mean Nusselt number is calculated as:

$$Nu = \left(\frac{Nu_{wall}+Nu_{bulk}}{2}\right)\frac{\lambda_{wall}}{\lambda_{bulk}} \tag{9}$$

,where Nu_{wall} and Nu_{bulk} are Nusselt numbers that are evaluated based on the thermophysical properties at the wall and bulk temperatures respectively. In each case, the Gnielinski correlation listed in equation (4) is applied to calculate the respective Nusselt number.

For the calculation of Re_{wall} in equation (4), it was found that the best fit was obtained by using the inlet velocity of CO_2 to compute the Reynolds number at the wall. As to the Re_{bulk}, it is calculated based on the local mean velocity. The mean velocity is calculated by some local parameters:

$$\dot{V}_{avg} = \frac{\dot{m}}{A\rho_{bulk}} = \frac{G}{\rho_{bulk}} \tag{10}$$

Based on a detailed numerical model developed by Pitla at al.[8-9], the effects of CO_2 mass flow rate and supercritical pressure on the heat transfer coefficient were predicted and shown in Figs. 4 and 5 respectively. As shown in Fig. 4, at a constant CO_2 gas cooler inlet temperature (395K) and pressure (10 MPa) and heat exchanger wall temperature (303K), the heat transfer coefficient significantly increases with higher CO_2 mass flow rates. In addition, for a fixed CO_2 mass flow rate, the heat transfer coefficient increases during gas cooling process until a maximum is reached. The maximum region in heat transfer coefficient is called the pseudocritical region around the pseudocritical point and coincides with the region where the specific heat has a maximum, as shown in Fig. 6 [10]. The pseudocritical point is defined as the temperature at which the specific heat becomes a maximum for a given pressure. The heat transfer coefficient then drops suddenly as the fluid enters the liquid regime. The pseudocritical temperature and maximum isobaric specific heat of CO_2 can be shown in Fig. 7.

Correspondingly, the pseudocritical temperature of CO_2 can be calculated with the following equation[11]:

$$T_{pc} = -122.6 + 6.124P - 0.1657P^2 + 0.1773P^{2.5} - 0.0005608P^3, \quad 75 \le P \le 140 \tag{11}$$

where the temperature (T_{pc}) and pressure (P) are in °C and bar, respectively.

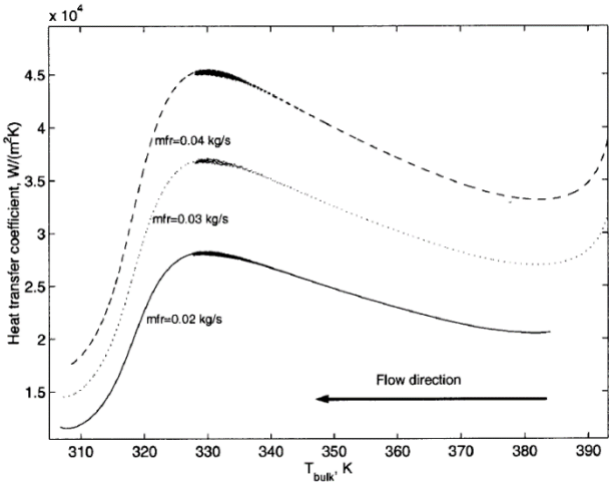

Fig. 4. The effect of mass flow rate on the heat transfer coefficient (T_{in}=395 K, P_{in}=10 MPa, T_{wall}=303 K)[6].

As depicted in Fig.5, the numerical model was also used to predict the effect of the CO_2 inlet pressure on the CO_2 heat transfer coefficient along its flow direction. To clarify, the CO_2 inlet temperature, mass flow rate and heat exchanger wall temperature were maintained at 390 K, 0.04 kg/s and 310 K respectively. The peak heat transfer coefficient value can be observed to shift to a higher temperature with increasing pressures. This coincides with the shift in the pseudocritical region to higher temperatures with an increase of pressure, as shown in Fig. 6. In addition, at higher pressures the variation in the heat transfer coefficient with temperature is smaller than at pressures near the critical point. This is due to the variation in thermophysical properties (specific heat) at maximum near the critical point, which decreases as the pressure increases from the critical pressure (7.353 MPa).

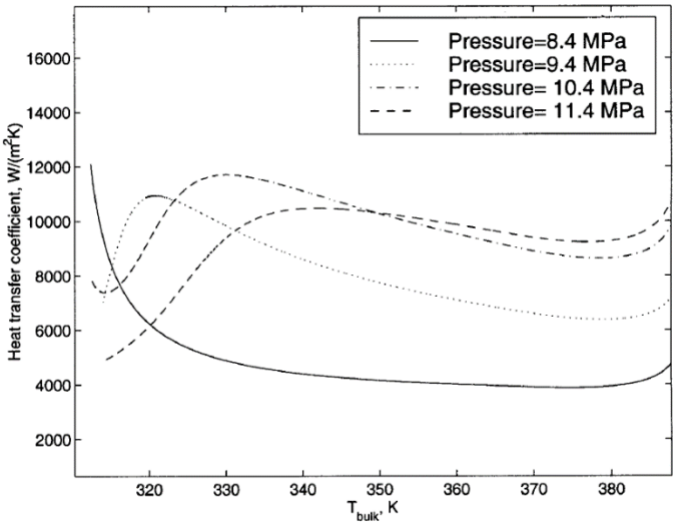

Fig. 5. The effect of pressure on the heat transfer coefficient (T_{in}=390 K, mass flow rate=0.04 kg/s, T_{wall}=310 K). [6].

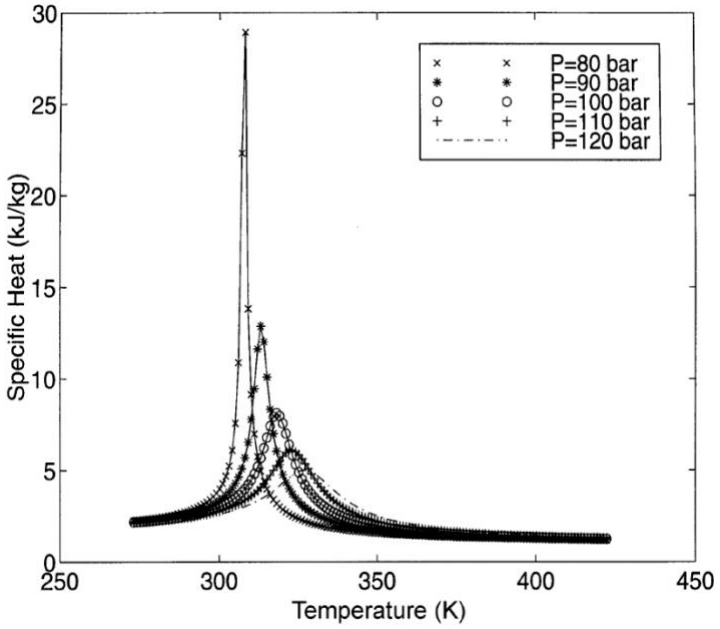

Fig. 6. Variation of CO_2 supercritical specific heat with temperature and pressure [10].

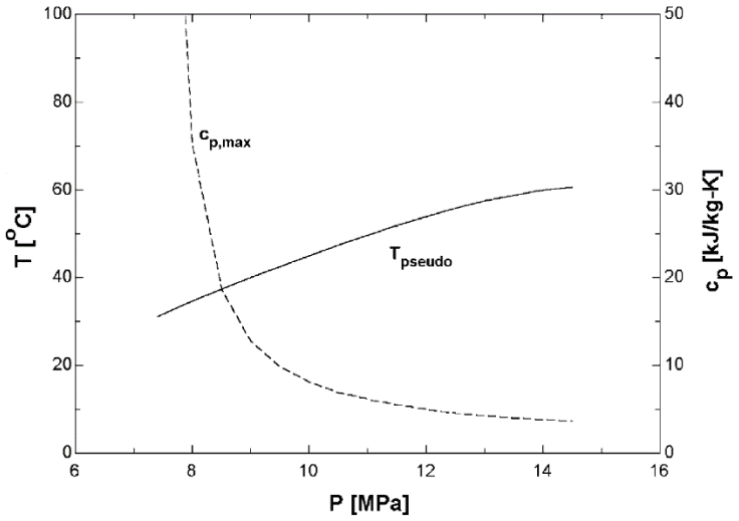

Fig. 7. Pseudocritical temperature and maximum isobaric specific heat of CO_2[11].

The Pitla correlation has been compared with measurements of a purposely built test rig[8]. For the experimental measurements, the tube inner diameter was 4.72mm, the CO_2 inlet and outlet temperature ranges were from 101°C to 134°C and 20°C to 34°C respectively, inlet pressure varied from 94 bar to 134 bar and CO_2 mass flow rates from 0.0196 kg/s to 0.0387 kg/s. It was found that 85% of the heat transfer coefficient values predicted by the correlation were within 20% accuracy when compared with the corresponding measurements. In addition, the correlation was also compared with three other existing correlations from literature [5][7][12] which found that the Pitla correlation was more accurate, particularly in the pseudocritical region when the pressure is relatively higher than the critical pressure.

Experimental investigations were carried out by Yoon et al. [13] to obtain the heat transfer and pressure drop characteristics during the CO_2 gas cooling process in a horizontal tube with an inner diameter of 7.73 mm. The tested CO_2 mass fluxes were fixed at 225, 337 and 450 kg $m^{-2}s^{-1}$ while the CO_2 pressures were controlled between 7.5 and 8.8 MPa which were close to the critical pressure. Accordingly, a simple formula for the heat transfer coefficient calculation was correlated:

$$Nu_{bulk} = aRe_{bulk}^{b} Pr_{bulk}^{c} \left(\frac{\rho_{pc}}{\rho_{bulk}}\right)^{n} \quad (12)$$

where, a=0.14, b=0.69, c=0.66, n=0 for $T_{bulk}>T_{pc}$

a=0.013, b=1.0, c=-0.05, n=1.6 for $T_{bulk}\leq T_{pc}$

Compared to the experimental data, the correlation can have an absolute average deviation of 12.7%.

5.3.2 Pressure drop

Since the flow of carbon dioxide in the supercritical gas cooling process is somewhat similar to that of a conventional single-phase flow, it seems reasonable to apply the single-phase pressure drop correlation in calculating the pressure drop during the cooling process. The frictional pressure drop for a fully developed turbulent single-phase flow in a smooth tube is calculated as:

$$\Delta P = f \frac{G^2 L}{2\rho D_i} \tag{13}$$

A number of equations have been developed for the friction factor, *f*. However, Blasius' equation [14] is the most widely used for the turbulent flow in smooth tube and is calculated as:

$$f = \begin{cases} 0.316Re^{-1/4} & for\ Re \leq 2 \times 10^4 \\ 0.184Re^{-1/5} & for\ Re > 2 \times 10^4 \end{cases} \tag{14}$$

As shown in Fig. 8, the pressure drop calculations with the Blasius' equation were compared with the measured pressure drop data to obtain an absolute average deviation about 4.9% [14]. The calculation with the Blasius' equation is therefore recommended for predicting pressure drop of CO_2 in the supercritical cooling process.

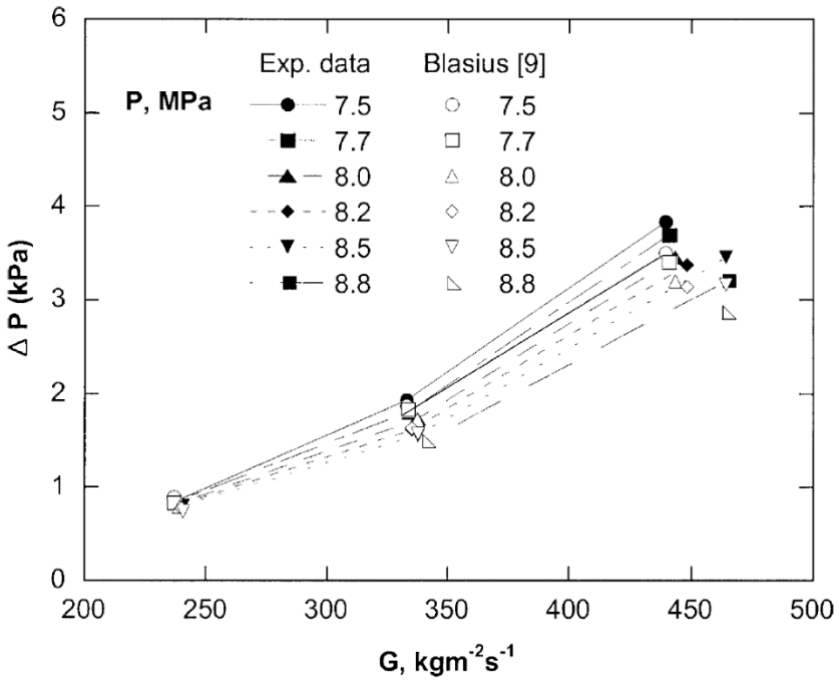

Fig. 8. Comparison of the measured pressure drop data with those predicted by Blasius' equation [14].

5.3.3. Calculations of smaller-diameter tubes

For smaller-diameter tubes such as microchannel, different correlations might be applied for the calculations of heat transfer and pressure drop during CO_2 supercritical cooling processes. The heat transfers during CO_2 supercritical cooling processes in 0.8 mm microchannel tubes were measured and correlated [15]. It was found that the standard single-phase correlations such as the widely used Dittus–Boelter model and the Gnielinski correlation [5] gave good correspondence between measured and calculated heat transfer coefficients. Meanwhile, the Colebrook and White correlation reproduced the pressure drop data well.

In addition, the heat transfer coefficients for CO_2 supercritical cooling processes in horizontal micro/mini tubes were measured[11]. Test tubes were stainless steel tubes with inside-

diameters of 0.5, 0.7, 1.1, 1.4, 1.55 and 2.16 mm, respectively. The pressures and temperatures measured ranged from 7.4 to 12 MPa and 20 to 110 °C, respectively. The buoyancy force significantly affected both supercritical CO_2 flow and heat transfer. However, the buoyancy effect became smaller as the tube diameter decreased. They reported that the existing correlations for larger tubes deviated notably from their test data for the micro/mini tubes. Based on the test data, they developed a correlation for the axially averaged Nusselt number with a mean relative error of 9.8%.

5.4 Modelling and performance evaluation

It is known that at a constant evaporating temperature the maximum cooling COP increases greatly with lower refrigerant temperature at the gas cooler exit. The temperature difference between the refrigerant outlet and incoming ambient air is known as approach temperature (AT) for an air-cooled gas cooler. The minimization of the approach temperature will greatly affect the system efficiency[16] , this being mainly dependent on the optimal design of the heat exchanger. Considering that circuit arrangements and structural parameters will affect the optimal design of the heat exchanger, an efficient and economical option would be to utilize the simulation technique for the optimal design.

In CO_2 transcritical cycles, finned-tube gas coolers are not as popular as aluminium minichannel heat exchangers, which have advantages of being light-weight and compact, with a lower risk of high-pressure stresses, and are already widely used in automobile air-conditioning. Therefore, a great deal of research and development effort has been put into minichannel heat exchangers [17–19]. However, because of the lower cost, the finned-tube coils are still believed to be competent types of gas coolers. Theoretically three modelling methods could be used in the performance analysis of such gas coolers: Effectiveness-NTU or LMTD, i.e. lumped method, tube-in-tube, and distributed method. Since there is a rapid change of CO_2 thermophysical properties with temperatures during an isobaric gas cooling process, it is not practical to use the overall Effectiveness-NTU or LMTD method to simulate gas coolers, particularly if the property profiles (such as temperature) need to be predicted[20]. The tube-in-tube method developed from the research of Domanski [21,22] was utilized in the simulation of a gas cooler by Chang and Kim [23]. By means of the model simulation, the effects of coil structural parameters on the performance of the gas cooler were investigated. It was found from the simulation results that the approach temperature can be reduced with an increased heat exchanger front area. Although the model demonstrates significant improvement with this method, a more detailed modelling strategy in the distributed method is still expected to further enhance simulation accuracy and therefore obtain more reliable conclusions.

5.4.1 Distributed method

The distributed method was used in developing the simulation model for finned-tube air-cooled CO_2 gas coolers [24]. A diagram with sub elements of the coil in a three-dimensional (3-D) space for the model is schematically drawn in Fig. 9. Tubes are arranged parallel to the *i* direction, *j* is specified in the longitudinal direction, while *k* is in the transverse direction. Air is flowing parallel to *j* direction and refrigerant is assumed to be in approximate counter-cross direction to air for this sample. The number selection of small elements in the *i* direction is arbitrary from one to infinity. The larger this value is, the more accurate the simulation will be, but expensive computing time will be sacrificed. The coordinate of each divided element in the 3-D space can then be determined. The coordinate value *i* represents the number of sub-elements for each tube selected by the model; *j* corresponds to tube row numbers in longitudinal paths starting from the air inlet, and *k* equals the tube numbers in the transverse path originating from the bottom. Therefore, the state point of either refrigerant or air at each specified sub-

element in the 3-D space can be positioned with its corresponding coordinate values *i, j* and *k*, which vary according to the circuit number and tube number. The tube number starts from refrigerant inlet to refrigerant outlet for each circuit. The solving routine firstly starts from the circuit loop if there is more than one circuit for the coil. For each circuit, the simulation will run through each numbered tube starting from the refrigerant inlet and then the element loop for each pipe. The whole modelling work depends on setting up the conservation equations for each sub-element and an efficient routine to solve these equations. The solutions for one sub-element can be used as the inputs for the next sub-division. The air side parameters for each element, which are unknown initially, will be assumed first. These parameters will be updated by next iteration. The total heating load of the gas cooler is calculated at the end of each iteration. The iteration will carry on until all the loops are cycled and the total heating loads for two continuous iterations are almost unchanged.

5.4.1.1 Refrigerant side conservation equations

Before setting up the refrigerant side conservation equations for each element, the following assumptions are proposed:

- System is in steady state.
- No heat conduction in the direction of tube axis and nearby fins.
- Air is in homogeneous distribution, that is, air-facing velocity to each element is the same.
- No contact heat resistance between fin and tube.
- At any point in the flowing direction the refrigerant is in thermal equilibrium condition.

Mass equation:

$$\frac{d}{dz}(\dot{m}_r) = 0 \tag{15}$$

Momentum equation:

$$\frac{1}{A_i}\frac{d}{dz}(\dot{m}_r u) = -\frac{dP}{dz} - \frac{\tau_{wi} s_{wi}}{A_{wi}} \tag{16}$$

Energy equation:

$$\frac{d}{dz}(\dot{m}_r h) = -(\pi\, d_o)\dot{q} \tag{17}$$

The above equations can be easily discretized as below for a sub-element shown in Fig. 9 with coordinate from (*i, j, k*) to (*i+1, j, k*). The dimensions of the sub-element at (*i, j, k*) directing to *i, j, k* are Δz_i , Δz_j and Δz_k respectively.

Mass equation: $$\dot{m}_r\Big|_{(i+1,\,j,\,k)} - \dot{m}_r\Big|_{(i,\,j,\,k)} = 0 \tag{18}$$

Momentum equation: $$\frac{1}{A_i}\left[(\dot{m}_r u)\Big|_{(i+1,\,j,\,k)} - (\dot{m}_r u)\Big|_{(i,\,j,\,k)}\right] = -\Delta P - \Delta P_f \tag{19}$$

where, $$\Delta P_f = f\,\frac{G^2 \Delta z_i}{2\rho\, d_i} \tag{20}$$

Energy equation:

$$(\dot{m}_r h)|_{(i+1,j,k)} - (\dot{m}_r h)|_{(i,j,k)} = -(\pi d_0)\dot{q} \times \Delta z_i \tag{21}$$

The conservation equations can also be applied for the airside calculation. The pressure drop calculation is used instead of the momentum equation and for this side, the heat transfer calculation is included in the energy equation. In addition, there is a heat balance between the air and refrigerant sides for each element.

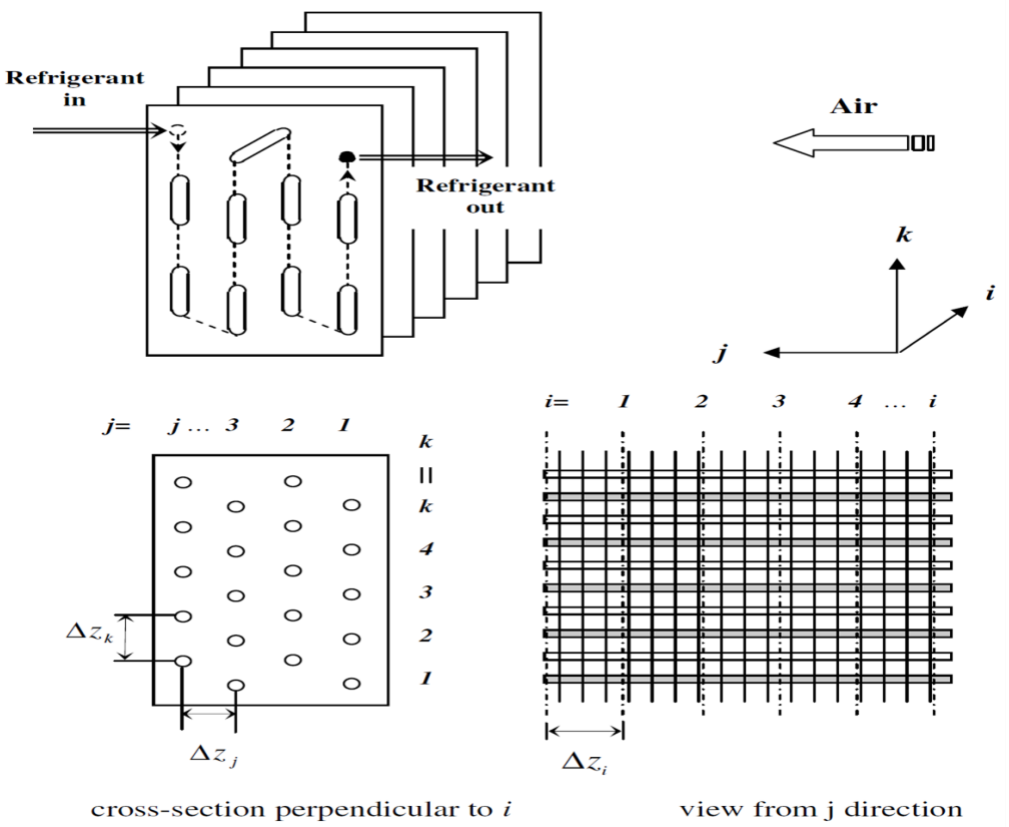

Fig. 9. Three-dimensional coordinate of sub elements in the coil for the gas cooler model

5.4.1.2 Airside Heat Transfer

Effectiveness-NTU method is used in the calculation of heat transfer for airside in one grid section.

$$\dot{Q}_a = \varepsilon C_{\min}[T_r(i,j,k) - T_a(i,j,k)] \tag{22}$$

where the effectiveness ε is calculated as below:

$$\varepsilon = 1 - \exp(-\gamma \frac{C_{\max}}{C_{\min}}) \quad \text{for } C_{\max} = C_h$$
$$\text{where } \gamma = 1 - \exp(-\frac{UA}{C_{\max}}) \tag{23}$$

and,

$$\varepsilon = \frac{C_{\max}}{C_{\min}}(1-\exp(-\gamma\frac{C_{\min}}{C_{\max}}))\ \ for\ \ C_{min}=C_h$$
$$where\ \ \gamma = 1-\exp(-\frac{UA}{C_{\min}}) \tag{24}$$

The product *UA* (overall heat-transfer coefficient times area) can be calculated as:

$$UA = (\frac{1}{\alpha_a \eta_0 A_0} + \sum R_i + \frac{1}{\alpha_r A_r})^{-1} \tag{25}$$

where ΣR_i is the sum of heat conduction resistances through the pipe wall and fin.

The heat transfer from airside can be calculated as:

$$\begin{aligned}\dot{Q}_a &= \dot{m}_a(i,j,k)\times Cp_a(i,j,k)\times[T_a(i,j+1,k)\\ &\quad -T_a(i,j,k)]\\ &= UA(i,j,k)\times[T_r(i,j,k)-T_a(i,j,k)]\end{aligned} \tag{26}$$

The parameters at grid points (*i+1, j, k*) for refrigerant and (*i, j+1 ,k*) for air can be obtained when equations (18) to (26) are solved together.

The accurate model prediction also relies on the precise calculations of fluid properties, heat transfer coefficients and pressure drops on both refrigerant and air sides. The CO_2 refrigerant properties are calculated using subroutines from the National Institute of Standards and Technology software package REFPROP [25]. For calculating the refrigerant heat transfer coefficient, the correlation from Pitla et al. is utilized [6]. The friction pressure drop is calculated in equation (20) and the Blasius equation [14] is used to calculate the friction factor *f*. The air side heat transfer and friction coefficients are computed using the correlations by Wang et al [26] [27].

5.4.2. Model validations

To develop a performance database for the component design in CO_2 transcritical cycles, a special designed test facility was set up by Hwang et al. [28]. The test system was composed of an air duct and two environmental chambers that housed an evaporator, a gas cooler, an expansion valve and a compressor. By means of this test rig, a set of parametric measurements at various inlet air temperatures and velocities, refrigerant inlet temperatures, mass flow rates and operating pressures were carried out on a specified CO_2 gas cooler. The side view of the circuit arrangement for the tested gas cooler is shown in Fig.10. The air flow is from right to left, and the refrigerant inlet is at the upper left numbered with “0”; the refrigerant outlet is at the lower right numbered with “54” for the heat exchanger. The dashed lines in the Figure indicate the U-bends of the rear side noted with odd numbers, while the solid lines signify the U-bends of the front side noted with even numbers. To measure the variation of refrigerant temperature along the heat exchanger pipes, numbers of thermocouples were attached on the outside surfaces of the front side U-bend pipes and at the refrigerant inlet and outlet as well. These thermocouples were well-insulated to get a more accurate measurement. The structural specification of the gas cooler is listed in Table 1.

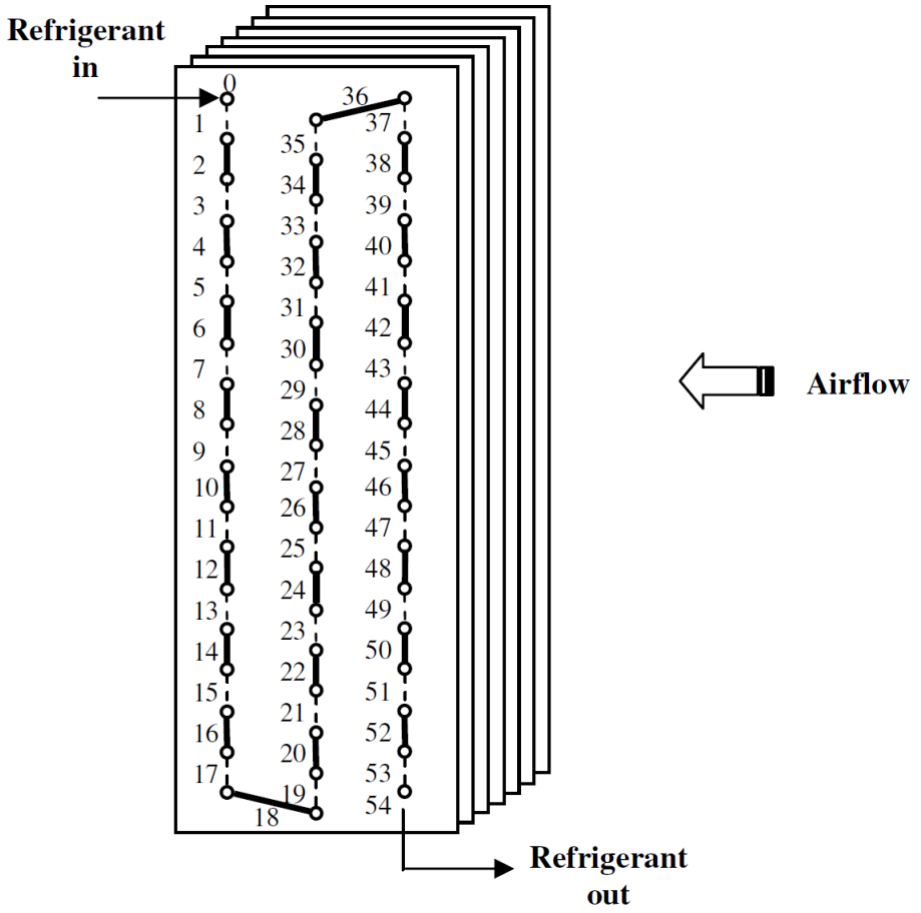

Fig. 10. Tested gas cooler with numbered pipes

The test conditions, 36 in total, are listed in Table 2. Each test condition contains the measurements of air inlet temperature, air velocity, refrigerant inlet temperature, refrigerant inlet pressure and refrigerant mass flow rate. These measurements and the coil structural parameters will be used as model inputs and parameters respectively. Therefore, the predicted refrigerant temperature profile at each test condition is compared with the corresponding test result in order to validate the model. To save space, comparison results for twelve test conditions with numbers 1 to 3, 10 to 12, 19 to 21 and 25 to 27, listed in Table 2, are selected and shown in Figs. 11 to 14 respectively. It can be seen from both simulation and test results that a sharp refrigerant temperature decrease occurs in the third pipe row (j=3), pipes numbered from 0 to 18 in Fig. 10. The temperature changing rates in the second (j=2) and first rows (j=1) are gradually reduced. In addition, at constant refrigerant pressures and mass flow rates, similar refrigerant inlet temperatures and unchanged air inlet temperatures, the refrigerant temperature at any specified location is always lower for higher front air velocity. This is because at higher front air velocities the heat transfer is enhanced. The predicted refrigerant temperature profile for each test condition matches well to the test result. To facilitate the comparison, the constant inlet air temperature line is also presented in each plot. For all of the test conditions, the refrigerant temperatures at the gas cooler outlet are predicted and compared with those of test results, as shown in Fig. 15. The temperature discrepancies between the simulation and test results for refrigerant outlet temperatures are mostly within ±2 °C when air front velocity is above 1m/s. Larger errors are predominantly caused when the air front velocity is at 1m/s. The correlation of airside heat transfer coefficient at lower air velocities therefore needs to be

further revised. The simulation can thus be concluded to fairly represent the test results and the model is therefore validated.

Table 1 Specification of the tested gas cooler

Dimension	
$W \times H \times D$ (m)	$0.61 \times 0.46 \times 0.05$
Front area (m^2)	0.281
Fin	
Shape	Raised lance
Fin pitch (mm)	1.5
Thickness (mm)	0.13
Tube	
Number of tubes row	3
Number of tubes per row	18
Tube outside diameter (mm)	7.9
Tube inside diameter (mm)	7.5
Tube shape	Smooth

Table 2 Test conditions

Test conditions	Air inlet air temperatures (°C)	Air velocity (m/s)	Refrigerant inlet temperature (°C)	Refrigerant inlet pressure (MPa)	Refrigerant flow rate (kg/s)	Tested refrigerant outlet temperature (°C)	Simulated refrigerant outlet temperature (°C)
1	29.4	1	118.1	9	0.038	40.4	38.0
2	29.4	2	109.5	9	0.038	33.5	33.5
3	29.4	3	113.5	9	0.038	31.3	31.5
4	29.4	1	124	10	0.038	41.5	36.9
5	29.4	2	118	10	0.038	32.3	31.2
6	29.4	3	117.1	10	0.038	31.1	30.3
7	29.4	1	128.8	11	0.038	40.4	34.3
8	29.4	2	123.5	11	0.038	31.7	30.4
9	29.4	3	123.1	11	0.038	30.9	29.9
10	35	1	121.3	9	0.038	43.1	40.6
11	35	2	119.4	9	0.038	39.8	38.8
12	35	3	118.8	9	0.038	38.2	37.9
13	35	1	127.7	10	0.038	45.5	41.9
14	35	2	122.6	10	0.038	38.7	37.9
15	35	3	122.2	10	0.038	37.2	36.6
16	35	1	133.3	11	0.038	46.0	40.9
17	35	2	128.9	11	0.038	38.0	36.6
18	35	3	128.4	11	0.038	36.7	35.6
19	29.4	1	94.8	9	0.076	41.1	41.1
20	29.4	2	90.8	9	0.076	38.4	38.8
21	29.4	3	86.9	9	0.076	37.2	37.8
22	29.4	1	103.3	10	0.076	45.8	44.9
23	29.4	2	94.8	10	0.076	39.1	40.4
24	29.4	3	90.7	10	0.076	35.3	37.5
25	29.4	1	110.6	11	0.076	49.3	47.0
26	29.4	2	100.7	11	0.076	38.4	39.5
27	29.4	3	97.1	11	0.076	33.9	35.6
28	35	1	92.5	9	0.076	43.8	43.3
29	35	2	90	9	0.076	40.2	40.9
30	35	3	88.4	9	0.076	39.4	40.0
31	35	1	104.1	10	0.076	48.0	47.2
32	35	2	98.4	10	0.076	43.4	43.6
33	35	3	93.9	10	0.076	41.1	42.0
34	35	1	109.6	11	0.076	51.5	49.7
35	35	2	101.9	11	0.076	43.6	44.3
36	35	3	98.4	11	0.076	40.5	41.6

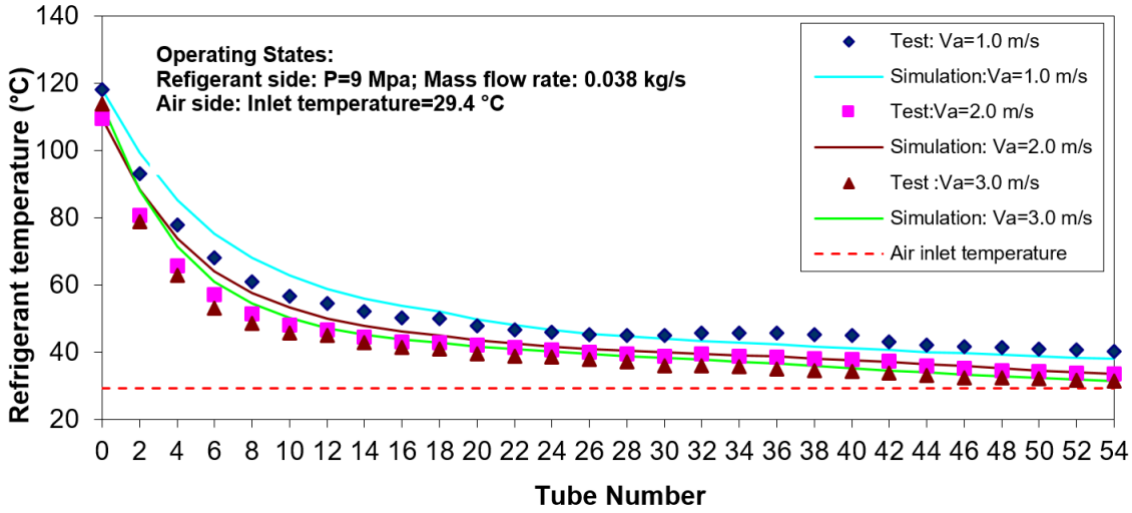

Fig. 11. Comparison of simulation with test results of test condition Nos. 1 to 3 for refrigerant temperature profile.

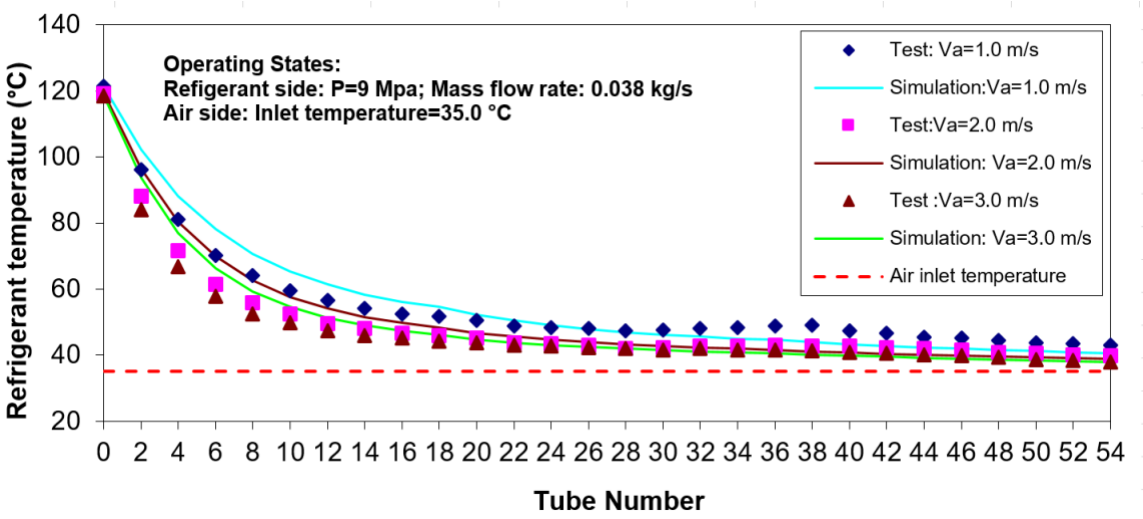

Fig. 12. Comparison of simulation with test results of test condition Nos. 10 to 12 for refrigerant temperature profile.

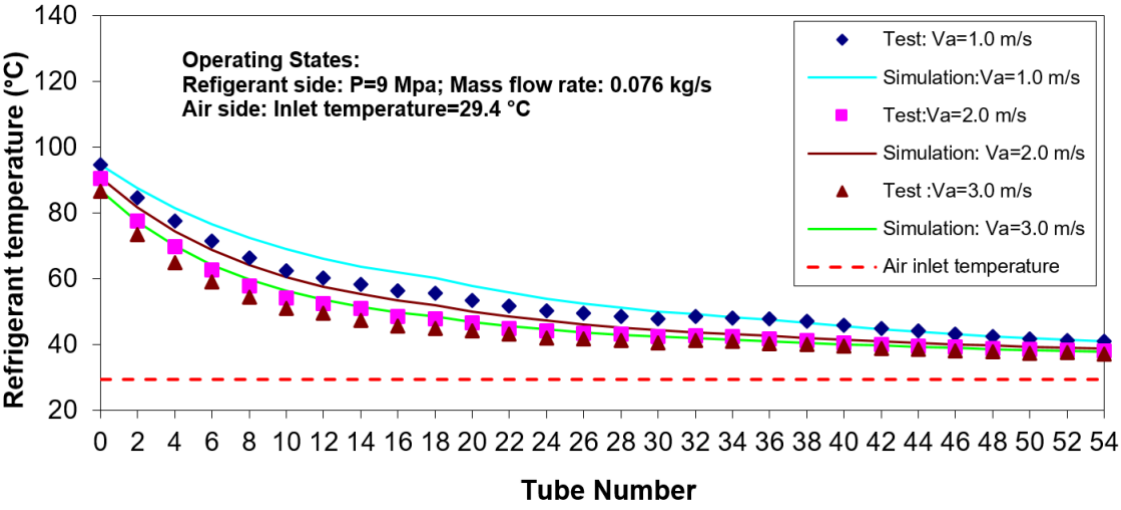

Fig. 13. Comparison of simulation with test results of test condition Nos. 19 to 21 for refrigerant temperature profile.

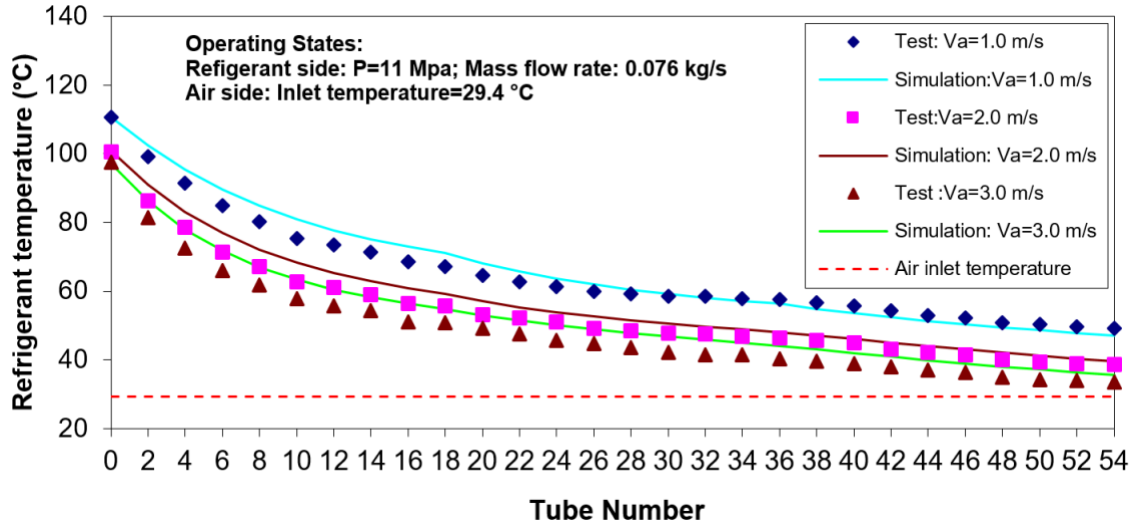

Fig. 14. Comparison of simulation with test results of test condition Nos. 25 to 27 for refrigerant temperature profile.

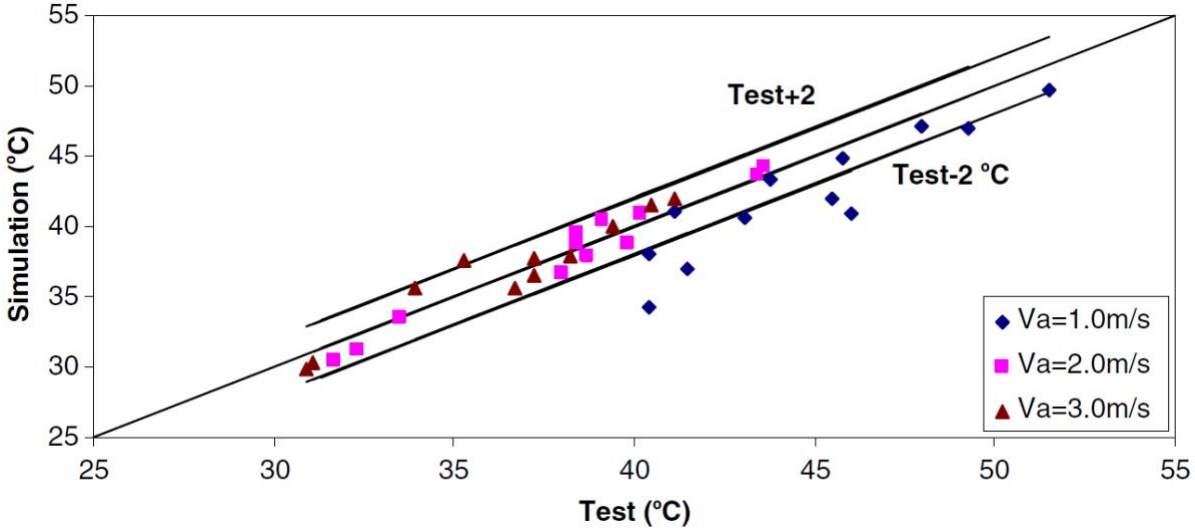

Fig. 15. Comparison of simulation with test results of all test conditions for refrigerant temperatures at gas cooler outlet.

5.5 Microchannel CO_2 gas coolers

It is known that CO_2 refrigeration, air conditioning and heat pump systems can be applied into commercial, residential and industrial purposes. Successful application of the CO_2-based technology depends on the development of efficient and compact components including the gas coolers with low weight, good reliability, and low cost, particularly in the application of automobile. Since 2008 in the EU, the focus on greenhouse effect of fluorinated compounds has led to a proposed gradual phase-out of refrigerant R134a in mobile air conditioning due to its relatively high Global Warming Potential (GWP). Subsequently, as one of the most significant applications, CO_2 air conditioning has been widely applied into automotive industries in which the mass and space requirements are of particular importance in mobile systems.

The first automobile air-conditioning gas cooler prototypes were developed and manufactured in 1990-1991[29]. At that time, mechanically expanded round-tube units were commonly used

in European cars, and a gas cooler was designed based on OD/ID 4.9 mm/3.4 mm aluminium tubes and plain aluminium fins. Core dimensions were based on the 1990 cross-flow condenser of a European passenger car [29]. The tube configuration and circuiting of the CO_2 unit are shown in Fig. 16. Core depths of the CO_2 and baseline unit were 34 mmm.

A problem in this first design was 'thermal short circuiting' due to heat conduction through the fins from hot tubes to colder tubes. The temperature gradient in the CO_2 supercritical gas cooling made this more important than with a condensing refrigerant. Thermocouples mounted on the tubes indicated that the refrigerant temperature actually increased towards the CO_2 gas cooler outlet as a consequence of conduction from the hot inlet tubes. The CO_2 gas cooler fins were then modified by a split (red dot line in Fig.16) between the second and third tube rows (in the direction of air flow). In addition, the refrigerant inlet was moved from centre row to rear row. Recorded tube-wall temperatures before and after this modification are shown in Fig. 17. Due to the high thermal conductivity of the tube-wall, the refrigerant temperature inside the tube is quite close to that of the tube-wall. The approach temperature was thus reduced from 12.2 K to 3.7 K, at an air-face velocity of 2.5 m/s. A reduction in air-face velocity to 1.0 m/s (and a reduction in compressor speed from 1600 to 700rev/min, i.e. to "idle" conditions) typically increased the temperature approach by 10-20% compared with normal driving conditions. The change in the gas cooler refrigerant inlet temperature in Fig. 17 is a result of the differences in evaporating pressure and compressor inlet temperature.

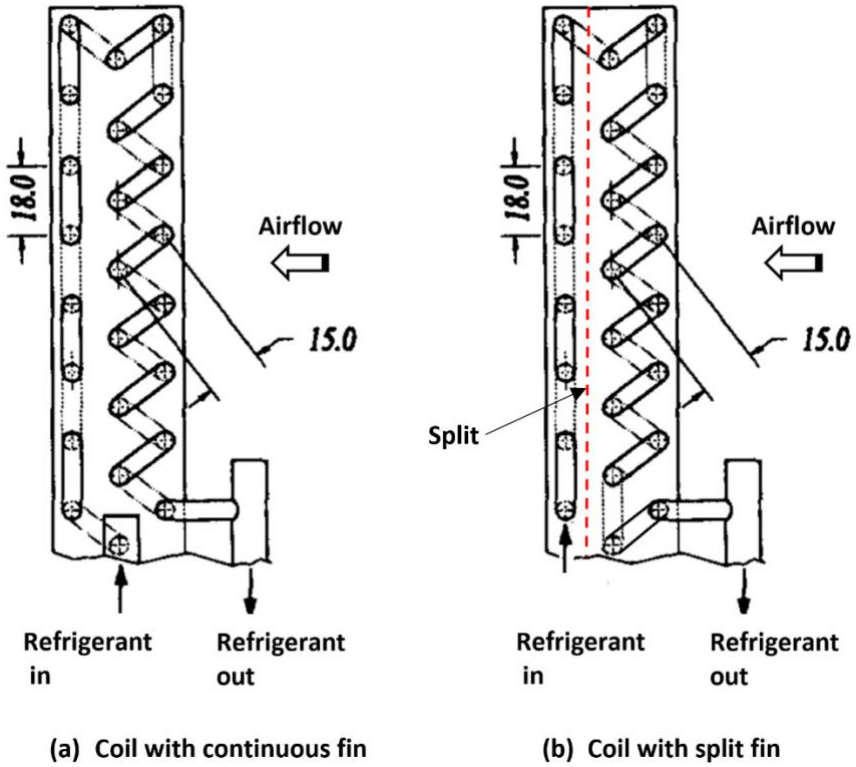

Fig. 16 Tube configuration and refrigerant flow in one (upper) of three equal circuits in a gas-cooler prototype (side view).Dimensions in mm.

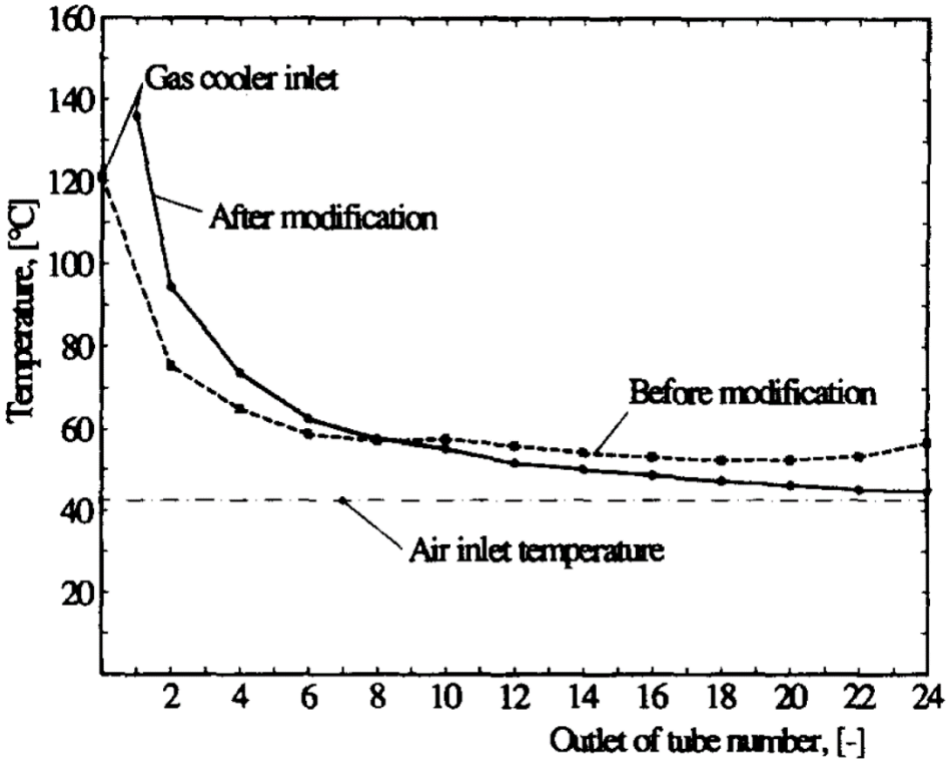

Fig. 17. Gas cooler tube-wall temperatures from refrigerant inlet to outlet. The temperature profiles before modification (dashed) and after introducing a split in the fin material between the second and third tube row (full line) are shown. Data recorded at 43°C air-inlet temperature and 2.5 m/s air-face velocity

Owing to the high-pressure level, large pressure drops can be tolerated in the gas cooler. Thus, heat exchangers can have refrigerant mass fluxes typically ranging from 600 to 1200 $kgm^{-2}s^{-1}$, with even higher numbers are reported for water-heating heat exchangers. The high working pressure and favourable heat transfer properties of CO_2 enable reduced tube diameters and small refrigerant-side surface areas. Since these reductions may give room for more air-side surface per unit core volume, their compactness can be increased. Table 3 gives examples of estimated heat transfer and pressure drop data for supercritical CO_2 flow in compact air-conditioning gas coolers, with tube diameters of 2.0 mm and 0.8 mm [15]. These dimensions are representative of round-tube and microchannel heat exchangers, respectively. As may be observed, the heat transfer coefficients are quite high for single-phase flow. Although the pressure gradient is higher for microchannel flow, the shorter circuits usually give lower overall pressure drops in this type of heat exchanger. Supercritical flow of CO_2 in microchannels is usually turbulent, although the transition regime may be encountered near the gas cooler outlet at low temperatures. Even though small-diameter round-tube heat exchangers can achieve low weight and compact design for a high-pressure fluid like CO_2, the added performance and compactness of brazed microchannel heat exchangers make these very attractive especially in transport applications.

Table 3 Estimated heat transfer and pressure drop data for supercritical CO_2 flow at 100 bar and 45°C[15]

	Diameter 2.0 mm	Diameter 0.8 mm
Mass flux ($kgm^{-2}s^{-l}$)	1000	800
Reynolds number	54400	17400
Pressure drop gradient[a] ($barm^{-l}$)	0.13	0.26
Nusselt number[b]	215	87
Heat transfer coefficient ($Wm^{-2}K^{-1}$)	6900	7000

[a]Assuming a tube roughness of 0.0015 mm (drawn tube)
[b]Based on the Dinus-Boelter correlation for cooled flow ($Nu = 0.023Re^{0.8}Pr^{0.3}$)

To handle the high pressures associated with the CO_2 cycle, many CO_2 systems employ heat exchangers with flat multiport (microchannel) tubes as shown in Fig. 18. This technology, with its folded louvered fins, provides additional benefits as a by-product. Compared to conventional flat-fin/round-tube designs, microchannel heat exchangers increase refrigerant-side area by about a factor of three, and have far less air-side pressure drops due to the streamlined profile presented by the tubes. The flat tubes enable higher face velocities that increase the air-side heat transfer coefficient.

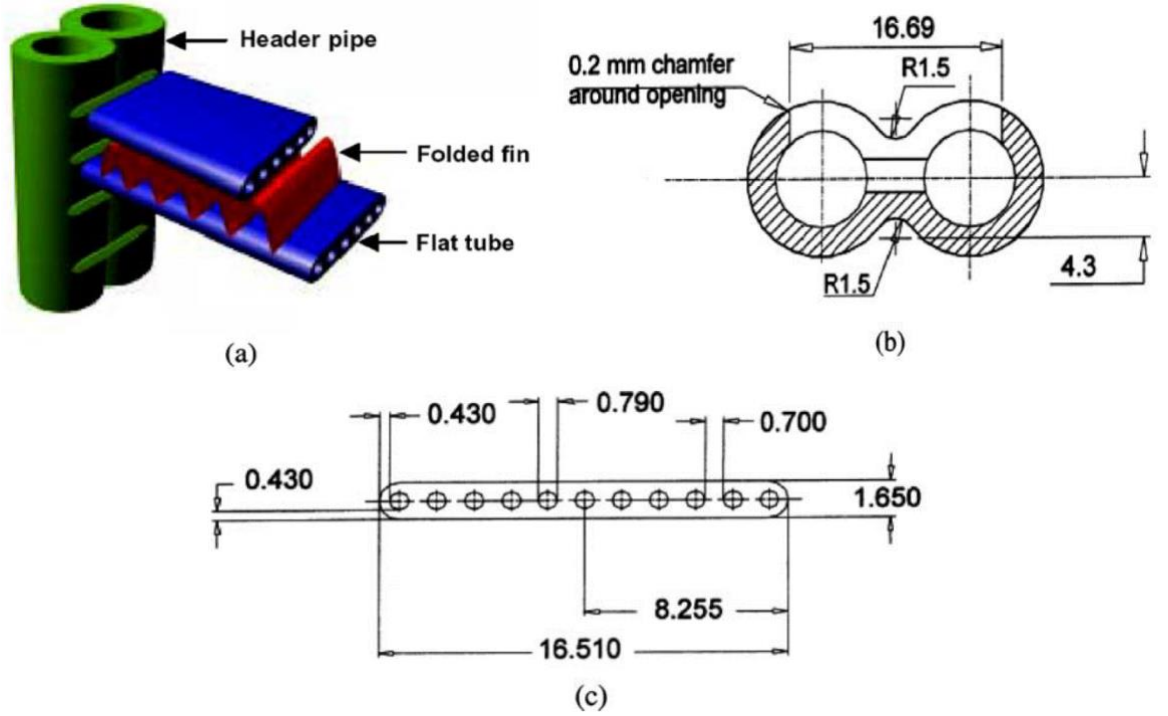

Fig. 18. A prototype microchannel CO_2 gas cooler for a car air conditioning system [19].
(a) Geometry of heat exchanger, (b) cross section of header pipe, (c) flat microchannel tube.

One issue in compact gas cooler design is internal conduction due to large temperature differences across small lengths. As pointed out by Pettersen et al. [19] internal conduction in fins, tubes and manifolds may lead to performance reduction. Solutions to avoid these problems include splitting of fins, use of several heat exchanger sections, and careful design of manifold geometries.

As indicated in Fig. 3, a CO_2 transcritical cycle is so sensitive to refrigerant exit conditions that a counter flow configuration is important for the gas cooler to exploit the large refrigerant-side temperature glide. Moreover, the steep refrigerant temperature glide allows for ideal cycle efficiency to be achieved at finite air flow rates, in contrast to the infinite air flow required to achieve ideal efficiency in the subcritical cycle.

Yin et al. [17] validated a gas cooler simulation model using measured inlet data for a diverse set of 48 operating conditions, predicting refrigerant outlet temperature within ±0.5 °C for most of the experimental data. They proposed a multi-slab gas cooler design (Fig. 19) and reported that the new design offered better performance than the commonly used multi-pass design (Fig. 19(a)). For the given heat exchanger volume, they reported that a newly designed cross-counter flow gas cooler could improve system capacity and COP by 3–4 and 5% respectively compared to the old design (Fig. 19(a)). The model was used to design the next-generation prototype gas cooler shown in Fig. 19(b), where a multi-slab overall counter flow configuration concentrates the cool air stream on the exiting refrigerant, because the transcritical cycle is so sensitive to this exit condition. The new gas cooler design achieves approach temperature differences of <2 °C at most operating conditions, because air flowing over the first slab undergoes only a small temperature change, and this ΔT is what places an upper bound on the approach temperature difference. The flat tubes are vertical in this prototype to facilitate condensate drainage and defrosting in heating mode. Finally, the refrigerant flows in a single pass from the inlet to outlet, with no intermediate headers, to accommodate reversibility and facilitate refrigerant distribution in heating mode. It is clear that flat tubes must be oriented vertically for any air-source heat pump, for reasons of defrost and condensate drainage, because both indoor and outdoor heat exchangers must function as evaporators as well as gas coolers.

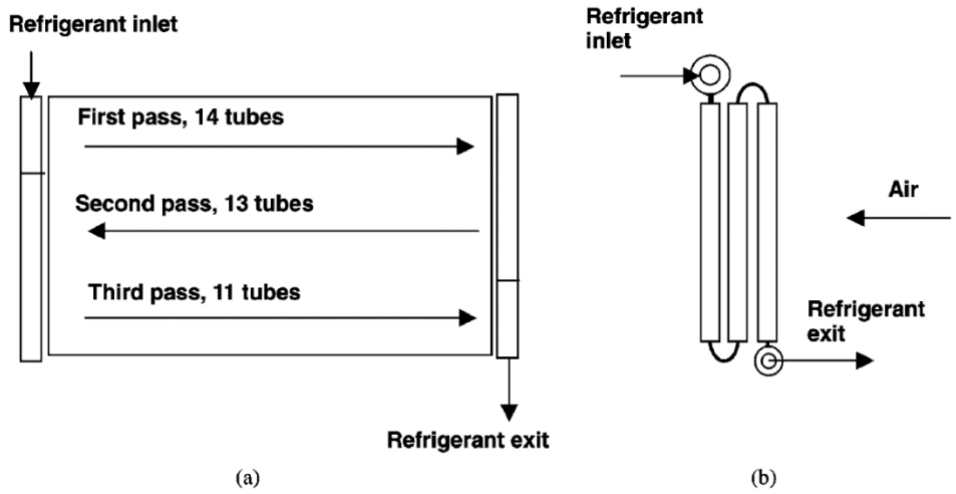

Fig. 19. Gas cooler design for a CO2 air-conditioning system [17]. (a) One-slab three-pass design, (b) three-slab one-pass design.

Conclusions and future work

As a main component, CO_2 gas cooler plays an important role to determine the system performance, compactness and cost. There exists an optimal heat rejection pressure during the gas cooler cooling process and it needs to be controlled properly to maximize the system COP. There are a number of operating parameters which can affect the optimal pressure but the most important and affective parameter is the refrigerant exit temperature of the gas cooler. It is

expected to have the lowest refrigerant exit temperature so as to obtain a higher COP at a lower operating pressure. The heat exchanger design and heat transfer and hydraulic behaviours during the cooling process are critical to determine the refrigerant exit temperature or approach temperature of the coil. There are a number of correlations from literatures to calculate the heat transfer coefficients of the CO_2 supercritical cooling processes. The correlation by Pitla is more suitable for the cooling process at the region a bit far away from the critical point while the correlation by Yoon is recommended for the calculation of cooling process close to the critical point. For the CO_2 pressure drop calculations, the conventional single-phase pressure drop calculation with the Blasius' equation can be applied. On the other hand, modelling strategy is an efficient and economical option for the heat exchanger optimal design. There are three modelling methods for the gas coolers including lump, tube-in-tube and distributed of which the distributed technique is more accurate and could present more detailed simulation results. In addition, for the application of automobile air conditioning, a better design option is to apply microchannel structure for the CO_2 gas cooler considering the particular requirement of compactness and cost. Furthermore, since there exists significant temperature difference during the CO_2 cooling process, the heat conduction through fins will affect negatively the heat exchanger performance. A better design solution to reduce the heat conduction is to apply split fins along the heat exchanger although an optimal design for the cutting fins is needed.

For the future work in this area, it is recommended that the CO_2 gas cooler designs need to be further optimised with both experimental and theoretical methods and integrated the components efficiently with their associated systems. More applications of the CO_2 gas coolers and their associated system are to be investigated and implemented.

Nomenclature

A	area (m^2)	*Subscripts*	
C_p	specific heat at constant pressure ($J\ kg^{-1}K^{-1}$)	a	air
C	capacity rate ($W\ K^{-1}$)	avg	average
d	diameter(m)	e	evaporator
D	depth (m)	ex	exit
f	friction factor	f	friction
G	mass flux ($kg\ m^{-2}\ s^{-1}$)	gc	gas cooler
h	enthalpy($J\ kg^{-1}$)	h	hot side
H	height (m)	*i*	inner, *i*th grid
i, j, k	coordinates	in	inlet
$\dot{m}$	mass flow rate ($kg\ s^{-1}$)	is	isentropic
P	pressure (Pa)	*j*	*j*th grid
$\dot{q}$	heat transfer per square meter ($W\ m^{-2}$)	*k*	*k*th grid
$\dot{Q}$	heat transfer (W)	min	minimum
R	resistance ($K\ W^{-1}$)	max	maximum
s	perimeter of inner pipe (m)	o	outer
T	temperature (K)	*opt*	*optimal*
u	velocity ($m\ s^{-1}$)	*pc*	*pseudocritical*
U	overall heat transfer coefficient ($W\ m^{-2}\ K^{-1}$)	r	refrigerant
Va, $\dot{V}$	air velocity ($m\ s^{-1}$)	sh	superheating
W	width (m)	wi	inner pipe wall
z	length (m)		

Greek symbol

α heat transfer coefficient (W m^{-2} K^{-1})

η efficiency

Δ difference

ρ density (kg m^{-3})

τ shear stress (N m^{-2})

ε effectiveness

References

[1] H. Inokuty, Graphical method of finding compression pressure of CO2 refrigerating machine for maximum coeffcient of performance, in: Proceedings of the 5th International Congress Refrigeration, Rome, 1928, pp. 185-192.

[2] J. Pettersen, G. Skaugen, Operation of trans-critical CO2 vapour compression circuits in vehicle air conditioning, in: Proceedings of the New Applications of Natural Working Fluids in Refrigeration and Air Conditioning, Hannover, Germany, 1994, pp. 495-505.

[3] S.M. Liao, T.S. Zhao, A. Jakobsen, A correlation of optimal heat rejection pressures in transcritical carbon dioxide cycles. Applied Thermal Engineering 20 (2000) 831-841.

[4] Man-Hoe Kim, Jostein Pettersen, Clark W. Bullard, Fundamental process and system design issues in CO2 vapor compression systems. Progress in Energy and Combustion Science 30 (2004) 119–174

[5] Gnielinski V. New equation for heat and mass transfer in turbulent pipe and channel flow. Int Chemical Engineering 1976;16:359–68.

[6] Srinivas S. Pitla, Eckhard A. Groll, Satish Ramadhyani. New correlation to predict the heat transfer coefficient during in-tube cooling of turbulent supercritical CO2. International Journal of Refrigeration 25 (2002) 887–895.

[7] Krasnoshechekov EA, Kuraeva IV, Protopopov VS. Local heat transfer of carbon dioxide at supercritical pressure under cooling conditions. Teplofizika Vysokikh Temperatur 1970;7(5):922–30.

[8] Pitla SS, Ramadhyani S, Groll EA. Convective heat transfer from in-tube flow of turbulent supercritical carbon dioxide: part 1—numerical analysis. Int J HVAC&R Research, Vol. 7, No. 4, October 2001, pp. 345–66.

[9] Pitla SS, Groll EA, Ramadhyani S. Convective heat transfer from in-tube cooling of turbulent supercritical carbon dioxide: part 2—experimental data and numerical predictions. Int J HVAC&R Research, Vol. 7, No. 4, October 2001, pp. 367–82.

[10] Pitla SS, Robinson DM, Groll EA, Ramadhyani S. Heat transfer from supercritical carbon dioxide in tube Flow: A Critical Review. Int'l J HVAC&R Research 1998;4(3): 281–301.

[11] Liao S, Zhao T. Measurements of heat transfer coefficients from supercritical carbon dioxide flowing in horizontal mini/meso channels. J Heat Transfer 2002;124:413–20.

[12] Baskov VL, Kuraeva IV, Protopopov VS. Heat transfer with the turbulent flow of a liquid at Supercritical Pressure in tubes under cooling conditions. Teplofizika Vysokikh Temoperatur 1997;15(1):96–102.

[13] Seok Ho Yoon, Ju Hyok Kim, Yun Wook Hwang, Mm Soo Kim, Kyoungdoug Min, Yongchan Kim. Heat transfer and pressure drop characteristics during the in-tube cooling

process of carbon dioxide in the supercritical region. International Journal of Refrigeration 26 (2003) 857–864.
[14] Incropera FP, DeWitt DP. Introduction to heat transfer. 3rd ed. New York: John Wiley & Sons; 1996.
[15] Pettersen J, Rieberer R, Leister A. Heat transfer and pressure drop characteristics of supercritical carbon dioxide in microchannel tubes under cooling. In: Groll EA, Robinson DM, editors. The Fourth IIR-Gustav Lorentzen Conference on Natural Working Fluids, West Lafayette, IN. 2000. p. 99–106.
[16] X. Fang, C. Bullard, P. Hrnjak. Heat transfer and pressure drop of gas coolers, ASHRAE Trans ,107(1), 2001, 255-266.
[17] J.M. Yin, C.W. Bullard, P.S. Hrnjak, R-744 gas cooler model development and validation, International Journal of Refrigeration, 24, 2001, 692-701.
[18]T.M. Ortiz, D. Li, E.A. Groll, Evaluation of the performance potential of CO_2 as a refrigerant in air-to-air air conditioners and heat pumps:system modeling and analysis, Final report, ARTI-21CR/610-10030, December 2003.
[19] J. Pettersen, A. Hafner, G. Skaugen, H. Rekstad. Development of compact heat exchangers for CO_2 air-conditioning systems, International Journal of Refrigeration, 21(3), 1998, 180-193.
[20] M.H. Kim, J. Pettersen, C.W. Bullard. Fundamental process and system design issues in CO_2 vapour compression systems. Progress in Energy and Combustion Science, 30, 2004, 119-174.
[21] P.A. Domanski, EVSIM-An evaporator simulation model accounting for refrigerant and one-dimensional air, NISTIR-89-4133. Washington, DC:NIST,1989.
[22] P.A. Domanski, D. Yashar, Optimization of finned-tube condensers using an intelligent system, International Journal of Refrigeration 30(2007) 482-488.
[23] Y.S. Chang, M.S. Kim. Modelling and performance simulation of a gas cooler for CO_2 heat pump system. V13,n3, HVAC&R Research, May 2007, 445-456.
[24] Y.T. Ge, R.T. Cropper. Simulation and performance evaluation of finned-tube CO2 gas coolers for refrigeration systems. Applied Thermal Engineering 29 (2009) 957–965.
[25]E.W. Lemmon, M.L. Huber, M. McLinden, NIST thermodynamic and transport properties of refrigerants and refrigerant mixtures- REFPROP, v8.0,
NIST Standard Reference Database 23 (2007).
[26] C.C. Wang, J.Y. Jang, N.F. Chiou, A heat transfer and friction correlation for wavy fin-and-tube heat exchangers, International Journal of Heat Mass Transfer 42 (1999) 1919–1924.
[27] C.C. Wang, W.S. Lee, W.J. Sheu, A comparative study of compact enhanced finand-tube heat exchangers, International Journal of Heat Mass Transfer 44 (2001) 3565–3573.
[28] Y. Hwang, D.D.H. Jin, R. Adermacher, J.W. Hutchins, Performance measurement of CO2 heat exchangers, ASHRAE Transactions (2005) 306–316.
[29]Lorentzen, G. and Pettersen, J., New possibilities for non-CFC refrigeration. In Proceedings of llR International Symposium on Refrigeration, Energy and Environment, Trondheim, Norway, 22-24 June 1992, pp. 147-163.